JOURNAL OF PETROLOGY | VOLUME 47 | NUMBER 6 | PAGES 1245–1254 | 2006 | doi:10.1093/petrology/egl010

Crystal Size Distributions Derived from 3D Datasets: Sample Size Versus Uncertainties

GUILHERME A. R. GUALDA*

DEPARTMENT OF THE GEOPHYSICAL SCIENCES, THE UNIVERSITY OF CHICAGO, 5734 S. ELLIS AVE., CHICAGO, IL 60637, USA

RECEIVED JUNE 23, 2005; ACCEPTED FEBRUARY 21, 2006
ADVANCE ACCESS PUBLICATION MARCH 22, 2006

Crystal size distributions (CSD) are the most commonly studied character in quantitative textural investigations of igneous rocks. The quality of CSD depends fundamentally on the sample size (i.e. total number of crystals). Here we use 3D X-ray tomographic datasets of two early erupted Bishop Tuff pumice clasts (comprising 849 and 446 quartz crystals) to investigate the effect of sample size on the quality of the quartz size distributions. Because CSD are obtained using a counting procedure, uncertainties related to counting statistics can be used as minimum estimates of error. Given that most natural samples are characterized by a decreasing number of crystals with increasing crystal size, uncertainties tend to increase markedly with crystal size, and the number of small crystals to be counted grows very quickly with increasing sample size. Accordingly, with as few as 100 crystals in total, it is possible to properly estimate the population densities for small size bins (20–80 μm). However, to obtain meaningful estimates across four bin sizes (20–320 μm), at least $\sim$250 crystals, but preferably $>$400 crystals are needed. To minimize the total number of crystals counted, and keep the uncertainties on the larger size ranges within reasonable values, it becomes necessary to study multiple volumes at variable spatial resolution.

KEY WORDS: *crystal size distributions*; *quantitative petrography*; *texture*; *X-ray tomography*

INTRODUCTION

It has long been recognized by petrographers that textures record fundamental information on the crystallization history of igneous rocks. Interestingly, however, petrography remained essentially qualitative until recently. The most notable exception is the quantification of modal compositions, which received considerable attention in the first half of the 20th century [see Chayes (1956) for a review]. A transition towards a more quantitative approach to the study of textures started only after the influential studies of Cashman & Marsh (1988) and Marsh (1988). Three main characters of textures are amenable to quantification: (1) the size distribution (Marsh, 1998), (2) the spatial distribution (Jerram *et al.*, 1996), and (3) the shape (Mock & Jerram, 2005) of crystals and vesicles.

Crystal and vesicle size distributions are the most studied of these characters, probably because they are clearly a function of nucleation and growth dynamics during igneous crystallization (see Marsh, 1988, 1998). For the most part, crystal size distributions are derived from observations in two dimensions, mainly from the study of thin sections and rock slabs. Studying the sizes and the distribution of crystals in three dimensions using observations on 2D sections imposes difficulties and limitations that have to be overcome by using stereological corrections (Sahagian & Proussevitch, 1998; Higgins, 2000).

As a result of these limitations, a full appreciation of the complexity and interpretative potential of the record represented by textures is best investigated using textural information obtained in three dimensions, as clearly shown by Mock & Jerram (2005). There are currently two main ways to obtain 3D images of rocks: serial sectioning (Bryon *et al.*, 1995; Cooper & Hunter, 1995) and X-ray tomography (Denison & Carlson, 1997), each with its own advantages and disadvantages [see Mock & Jerram (2005) for a discussion]. In very special circumstances, confocal microscopy can also be

*Corresponding author. Telephone: +1-773-702-8101. Fax: +1-773-702-9505. E-mail: ggualda@uchicago.edu

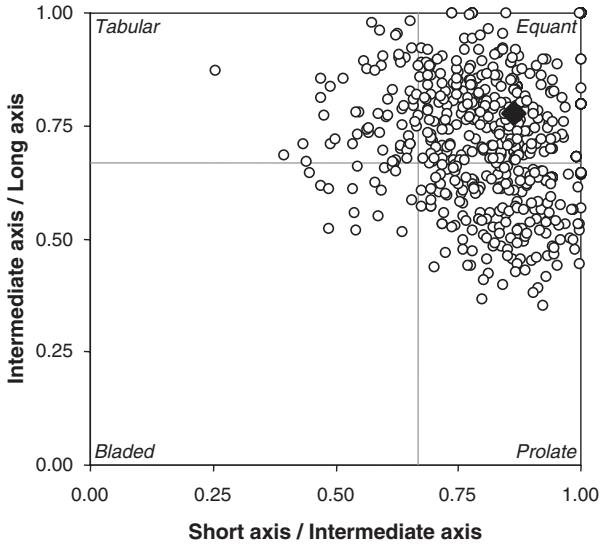

Fig. 1. Zingg diagram (short axis/intermediate axis vs intermediate axis/long axis) showing the distribution of shapes in sample F7-14B. Approximately 68% of the crystals fall in the equant field. Black diamond corresponds to the average ratios, corresponding to an axial ratio of 6:7:9.

employed to derive 3D datasets (Petford *et al.*, 2001; Castro *et al.*, 2003).

Using serial sectioning, Mock & Jerram (2005) investigated the texture of megacrysts in a porphyritic rhyolite. In that study, they performed two critical tests. First, they compared the results obtained in 3D ('true' results) with results obtained by sectioning through the analyzed volume, and showed that variations in grain shape place strong limitations on the quantitative study of textures using 2D sections. They also showed that crystal size distributions obtained with a subvolume composed of 200 or more crystals properly approximate the 'true' crystal size distribution.

In the course of a study of the textures of Bishop Tuff pumice clasts, we obtained 3D datasets—in many ways comparable with that of Mock & Jerram—using X-ray tomography (Gualda & Rivers, 2006). Two datasets are notable for the large number of crystals they contain, one with 849 quartz crystals (Sample F7-14, Run B; see Gualda & Rivers, 2006), and another with 446 quartz crystals (Sample F7-12, Run B). These datasets can be used to further evaluate the findings of Mock & Jerram (2005). In contrast to the Halle rhyolite studied by Mock & Jerram, quartz crystals in the Bishop Tuff samples we have studied so far are mostly equant (Fig. 1), such that it is expected that the effects of sectioning will be satisfactorily approximated by stereological corrections. However, because the studied pumice clasts are crystal poor (i.e. low number density), the study of pumice texture using 2D sections is inadequate. Hence, we do not try to test the effects of 2D sectioning in the evaluation of crystal size distributions in this study.

On the other hand, the more limited variation in crystal shape observed in the Bishop pumice clasts makes our dataset ideal to explore the effect of sample size (i.e. total number of crystals) on the quality of crystal size distributions derived from 3D datasets, and this is the focus of the present study. This is an important test, especially because the crystal populations in Bishop Tuff pumice clasts and in the Halle rhyolite differ in their characteristics and crystallization history. The analysis developed here expands on the treatment of Mock & Jerram (2005) in that we use counting statistics to give minimum estimates of the uncertainties associated with crystal size distributions.

SAMPLE DESCRIPTION, DATA ACQUISITION AND PROCESSING

The samples studied here are pumice clasts from the early erupted Bishop Tuff, fall unit F7 (Wilson & Hildreth, 1998). The bulk pumice density and the crystal contents were studied using a crushing and sieving technique (Gualda *et al.*, 2004), and the results were shown to agree well with those obtained using X-ray tomography (Gualda & Rivers, 2006). With bulk density and crystal contents of 634 kg/m^3 and 9·3 wt % crystals, Sample F7-14 has characteristics that are most typical of the early erupted Bishop Tuff pumice clasts studied by Wallace *et al.* (1999), Anderson *et al.* (2000), and Gualda *et al.* (2004). Sample F7-12 has lower density and crystal contents (499 kg/m^3 and 6·6 wt % crystals), but is also within the range investigated by previous workers [see Gualda *et al.* (2004) for a discussion].

Tomographic data were obtained using the GSECARS beamline at the Advanced Photon Source, Argonne National Laboratory, using a 22 keV beam. The samples were cut into cylinders of ~5 mm diameter and height, which were rotated at 0·5° steps until half a revolution was completed (i.e. 360 steps). Data were reconstructed into 3D maps of X-ray attenuation coefficients using procedures described in detail elsewhere [see Rivers *et al.* (1999) and references therein]. The resulting images are composed of voxels (volume elements) with ~7·8 μm in each linear dimension. Further details have been given by Gualda & Rivers (2006).

To obtain crystal size data, the resulting 3D maps have to be classified (i.e. each voxel in the image has to be assigned to a given phase) and individual touching objects have to be separated from each other (for details, see Ketcham, 2005; Gualda & Rivers, 2006). Both of these steps, as well as measurements of crystal properties, were performed using Blob3D (Ketcham, 2005).

The 3D distribution of the quartz crystals in the sample can be visualized using routines written by the author

Fig. 2. Three-dimensional view of the crystals in sample F7-14B. Quartz crystals are shaded black; sanidine crystals are dark gray; magnetite is light gray. Glass and vesicles were suppressed for clarity. Field of view is ~8 mm × 7 mm. An animated version of this figure is available at http://www.petrology.oxfordjournals.org.

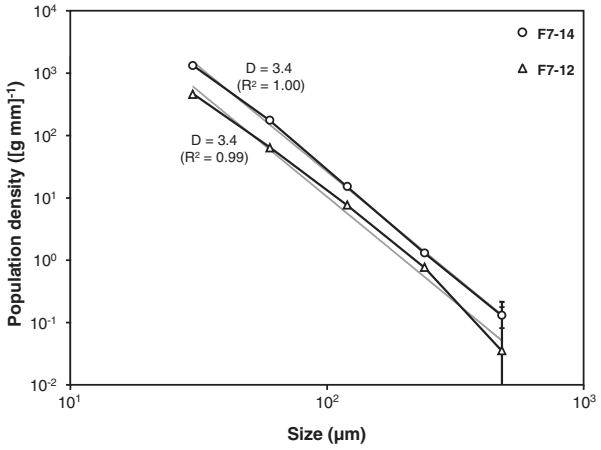

Fig. 3. Log–log plot showing the quartz size distributions for samples F7-14 and F7-12. In plots like this, power laws correspond to straight lines (gray), and the fractal dimension D is simply the slope of this line (or the exponent of the power law equation). It can be seen that the size distributions are well approximated by power laws, and the fractal dimension D is indicated in both cases. The size distributions were plotted using data from Gualda & Rivers (2006), and correspond to a combination of tomographic data collected at two resolutions, run A (17·1 μm voxel size) and run B (7·8 μm voxel size) [see Gualda & Rivers (2006) for a detailed discussion].

using IDL (Interactive Data Language, RSI), both as individual projections (Fig. 2), and as animations (Movie 1, online supplementary material available from www.petrology.oxfordjournals.org).

Quartz size distributions in these samples have been discussed in detail by Gualda *et al.* (2004) and Gualda & Rivers (2006). In those studies, we have argued that the concave upward shape of the quartz size distributions in semi-logarithmic plots is a function of crystal fragmentation. This is further indicated by the linear trends observed in log–log plots (Fig. 3), showing that the size distributions are fractal in character, and can be described by power laws of exponent −3·4, a situation very similar to that reported by Bindeman (2005) for Mt. Pinatubo pumice clasts.

Furthermore, we have shown that many quartz fragments are coated by glass, which indicates that fragmentation was at least partly magmatic in origin (Gualda *et al.*, 2004). It is also important to emphasize that the image processing techniques implemented in Blob3D allow fragments sitting close together be treated as a single crystal. Because we are studying only pumice clasts, the effects of transport processes below the glass transition temperature are unimportant, such that the fragment size distributions presented here are representative of the fragmentation state prior to eruption, possibly also affected by fragmentation in the early stages of the eruption process, as suggested by Pallister *et al.* (1996) for Mt. Pinatubo pumice clasts.

In all crystal size distribution plots shown here, the population density is cast in a per mass basis, i.e. number of crystals per mass of pumice, divided by the bin size [yielding units of $(\mathrm{g\ mm})^{-1}$], instead of the more usual per volume basis (mm^{-4} units). The reason for this choice relies on the fact that pumice volume is dominated by porosity, and it is to a great extent controlled by the eruptive history, such that it becomes an inadequate quantity to normalize the data to. Although the volume of dense rock could be used, there are two main advantages in using the mass of the pumice as the normalizing quantity: (1) whereas the mass of a pumice sample can be directly and easily determined, the volume of dense rock depends on knowledge of density and crystal contents, which are more difficult to determine; (2) calculation of the dense rock volume usually assumes no pre-eruptive bubbles, which may not have been the case for the Bishop magma (Gualda & Anderson, 2005), and, in such case, is directly correlated to the mass.

DATA ANALYSIS

To investigate the effects of sample size on the quality of the resulting crystal size distributions, we subdivided

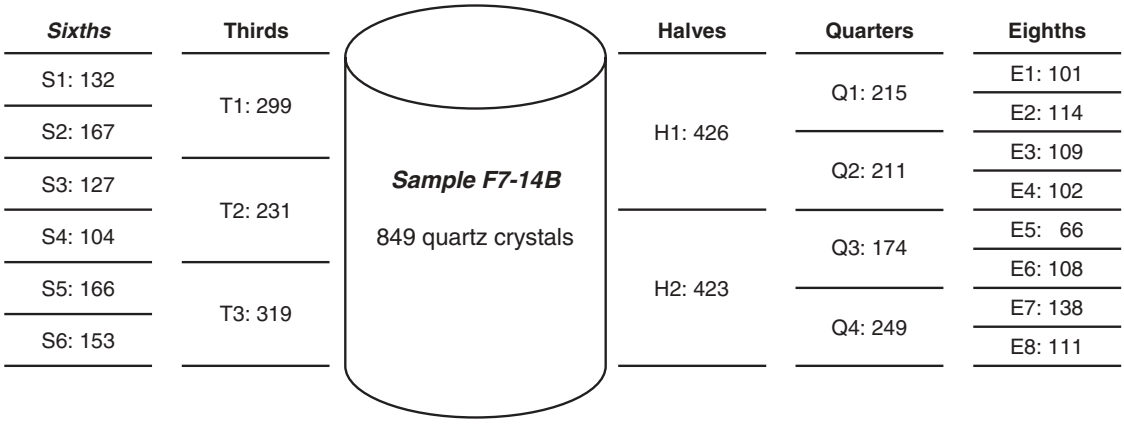

Fig. 4. Schematic representation of the procedure used to study the variation in the quality of quartz size distributions by successive splitting of the whole volume into subvolumes of the same thickness. Number of quartz crystals per volume fraction for sample F7-14B is indicated. It can be seen that with the exception of eighths E5 and E7, the number of quartz crystals per eighth is close to the expected value of 105.

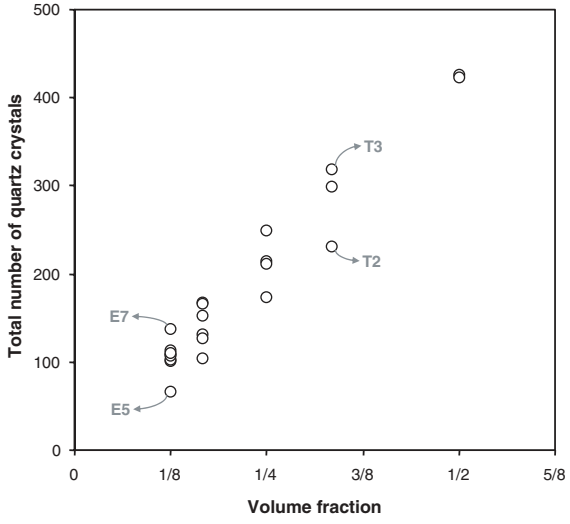

Fig. 5. Volume fraction vs total number of quartz crystals, showing the approximately linear increase in total number of crystals with sample volume for sample F7-14B. Eighths E5 and E7, whose crystal contents depart significantly from the average, are indicated. It should be noted that subvolumes that include either of these two eighths tend to show total crystal numbers departing from the average (e.g. thirds T2 and T3).

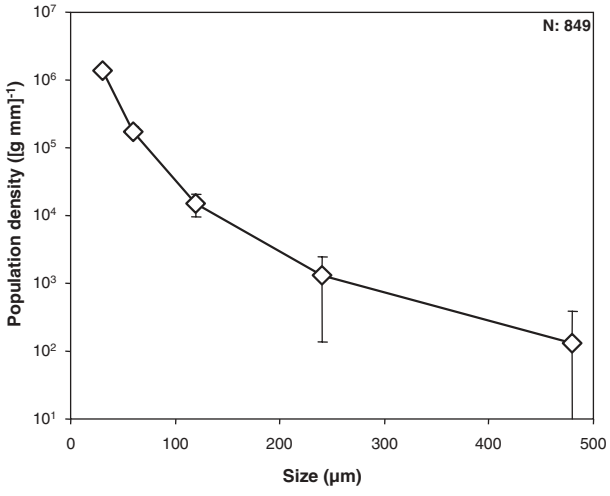

Fig. 6. Quartz size distribution for the whole volume for sample F7-14B, including a total of 849 quartz crystals. Population density is presented here on a per mass basis (rather than per volume) because of the vesiculated nature of the glassy matrix in pumice clasts. Error bars correspond solely to counting statistics. It should be noted that the curvilinear shape makes it inadequate to fit a straight line to the data points.

the original analyzed volumes into fractions, leading to sets of equivalent subvolumes (Fig. 4). The results for sample F7-14B, the most crystal-rich, are discussed in detail below, and are then compared with those for sample F7-12B.

In Fig. 4, the number of quartz crystals in each subvolume of sample F7-14B is indicated. As expected, the reduction in volume is accompanied by a decrease in the total number of quartz crystals (Fig. 5). It can also be seen that the number of crystals per eighth of the volume is relatively constant and close to the expected value of ~105; this shows that quartz crystals tend to be uniformly distributed in the sample. The most notable exceptions are eighth E5, with 66 quartz crystals, and eighth E7, with 138 crystals; consequently, the other subvolumes that include either of these eighths also show values for the total number of quartz crystals that depart from the expected average (compare, for instance, thirds T1, T2 and T3; Fig. 5).

The crystal size distribution for sample F7-14B is shown in Fig. 6 in a semi-logarithmic plot of population density vs size. The bin sizes in Fig. 6 were chosen in a manner similar to the phi scale used by sedimentologists. A somewhat arbitrary value of 20 μm was chosen as the

lowermost value, and the boundaries between bin sizes were chosen to be twice the previous value. This progressive increase in bin size is necessary because the number of crystals per size bin decreases rapidly, and size intervals with no counts are to be avoided. Although the choice of the lowermost value is usually immaterial, in this case, crystals of ~20 μm correspond to 3 voxels in diameter, such that they cannot be properly quantified, and have been automatically removed during image processing (see Gualda & Rivers, 2006).

The categorization of the data into size bins converts the construction of size distributions into a counting procedure, in which each class is characterized by its number of objects. In this case, uncertainties can be estimated based on the statistics of the Poisson distribution. Because the standard deviation of the Poisson distribution is simply $\sqrt{N}$, confidence intervals at the 95% level are usually computed as the value $\pm 2\sqrt{N}$. This is an approximation based on the central limit theorem (Howarth, 1998), and is strictly appropriate only for 'large' values of N (e.g. >25). As N becomes small, the confidence interval becomes more asymmetric; this is particularly important for $N < 4$, in which case the lower limit of the confidence interval calculated using the simplification becomes negative. Unfortunately, calculation of more appropriate limits is somewhat cumbersome (see Howarth, 1998). Because the confidence intervals for values of $N < 5$ are so large, the choice of calculation procedure is almost immaterial for practical purposes. Hence, for simplicity, we use here the simplified calculation (i.e. $2\sigma = 2\sqrt{N}$), and simply truncate the confidence intervals to avoid negative or zero numbers. It is important to note that these uncertainties correspond simply to uncertainties related to counting statistics, and have to be considered as minimum estimates of the actual errors.

To analyze the effect of decreasing sample size on the quality of the crystal size distribution obtained, we can compare the 'true' quartz size distribution with those calculated using each one of the subvolumes (Fig. 7).

With only two exceptions, the population density values for crystals smaller than 160 μm are within error of the 'true' values. The two exceptions correspond to the subvolumes with the smallest (eighth E5) and the fourth smallest (sixth S4) numbers of quartz crystals, 66 and 104, respectively (note that S4 includes E5). It should be emphasized that the error bars shown in Fig. 7 are for the 'true' size distribution, and are significantly smaller than the uncertainties related to counting statistics for the subvolumes, which were omitted for clarity; in any case, with as few as 100 crystals, the population density of crystals of <160 μm diameter can be estimated appropriately.

For crystals in the size range 160–320 μm, only with more than 400 crystals are the estimates systematically within error of the 'true' values, but estimates within error are obtained for samples with as few as 231 crystals (third T2). Samples with less than ~200 crystals yield poor estimates of the population density in the 160–320 μm size range.

It is not surprising that the population density for the size range 320–640 μm cannot be properly estimated even with sample sizes of ~400 crystals, given that only one such crystal is present in the whole volume (Table 1). As the error bars in Fig. 6 indicate, even the estimates using the whole dataset are to be considered only rough estimates.

It is convenient to use best-fit curves to describe crystal size distributions based on a small number of parameters. For instance, linear crystal size distributions are particularly common (e.g. Marsh, 1998), and can be described by two parameters (i.e. slope and intercept). It has already been shown that the fragment size distributions discussed here can be well approximated by power law equations (Fig. 3), yielding fractal dimensions of 3·4. One appropriate question is how well can the subvolumes reproduce this value. The values for the fractal dimension (D) calculated using each one of the 23 subvolumes, as well as that calculated using all 849 crystals, are plotted against the number of crystals in each subvolume in Fig. 8a (sample F7-14B). The plot shows relatively large scatter in the values of D for sample size smaller than ~200 crystals; for samples with $N > 200$, all but one value are within the range 3·0–3·5. As pointed out above, however, the population density for the size fractions 160–320 and 320–640 μm are characterized by relatively large uncertainties, and much of the scatter seen in Fig. 8a is due to the disproportionately large influence of these two values in the calculation of D, as is clearly illustrated by half H1. To minimize this effect, values of D were recalculated using only the size bins 20–40, 40–80, and 80–160 μm (Fig. 8b). As expected, the scatter in Fig. 8b is much reduced, and all subvolumes with N greater than ~250 (T1, T2, T3, H1, H2) provide excellent estimates (i.e. within 2%) of the fractal dimension D obtained calculated using the whole volume. Furthermore, all subvolumes with $N > 100$ provide estimates of D within 10% (within the range 3·0–3·5) of the 'true' value.

Analysis of the data for sample F7-12B (Fig. 9) reinforces the results outlined above. Values for the population density in all size fractions are within uncertainty for subvolumes with N larger than ~100. Also similarly, the fractal dimension is well estimated (within 5%) with sample size larger than ~200 crystals. This coincidence is not surprising, especially considering the similarity between the size distributions for the two samples. It is noteworthy that Mock & Jerram (2005) also found that 200 or more crystals were needed to properly characterize the crystal size distributions for the Halle rhyolite.

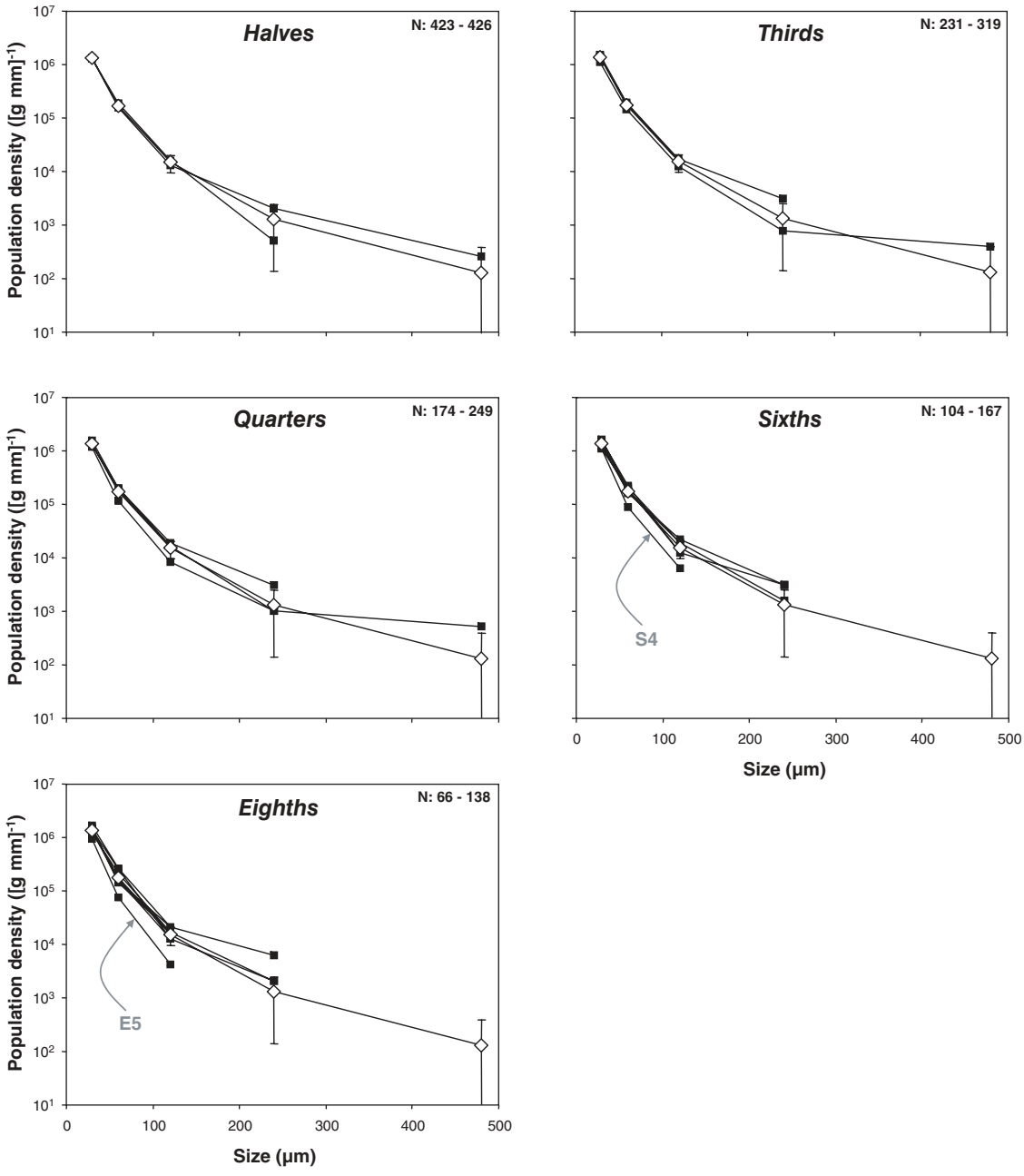

Fig. 7. Quartz size distributions for sample F7-14B obtained using the subvolumes shown schematically in Fig. 4. Black squares correspond to the quartz size distributions obtained with the subvolumes. Open diamonds and error bars correspond to the size distribution obtained with the whole volume. Numbers indicated in each diagram correspond to the range of total number of quartz crystals in the crystal size distributions shown. Sixth S4 and eighth E5, which are significantly distinct from the size distribution for the whole volume, are indicated.

DISCUSSION

Embodied in the above discussion are the facts that (1) the number of crystals in a given size range decreases dramatically with increasing crystal size, and (2) crystal size distributions are obtained using a counting procedure. Hence, for a given size interval, the uncertainties decrease as sample size increases according to a power law function of exponent close to −0·5 (Fig. 10). Also, comparison of uncertainties across size intervals clearly shows the effect of the decreasing number of crystals in the larger size intervals (Fig. 10).

The above discussion emphasizes the fact that there is no unique answer to the question of how many crystals are necessary to properly characterize a crystal size distribution. Intrinsically, the answer depends on the overall

Table 1: Number of crystals, population density, and uncertainties for each of the size fractions of sample F7-14B as counted for the whole sample volume

Bin (μm)	*N*	*n* [(g mm)$^{-1}$]	Uncertainty (2σ)	Relative uncertainty (%)
20–40	646	$1{\cdot}34 \times 10^{6}$	$1{\cdot}06 \times 10^{5}$	8
40–80	168	$1{\cdot}75 \times 10^{5}$	$2{\cdot}70 \times 10^{4}$	15
80–160	29	$1{\cdot}51 \times 10^{4}$	$5{\cdot}60 \times 10^{3}$	37
160–320	5	$1{\cdot}30 \times 10^{3}$	$1{\cdot}16 \times 10^{3}$	89
320–640	1	130	260	200

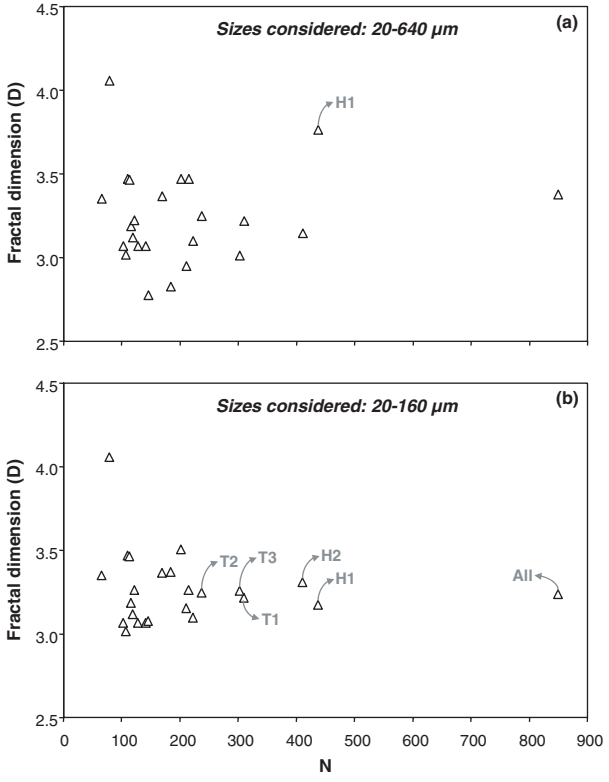

Fig. 8. Variation in the calculated fractal dimension (D) as a function of sample size (*N*) for all 23 subvolumes and for the whole volume for sample F7-14B. In (a), the whole range of crystal sizes (20–640 μm) was used, whereas in (b) only crystals within the range 20–160 μm were used. The difference between the two figures reflects the strong influence of the larger size fractions (160–320 and 320–640 μm) on the calculated D; because these larger size fractions are characterized by significantly larger uncertainties, scatter in (b) is much reduced. The value of D is adequately assessed for samples with more than 100 crystals, and D is very well estimated for all samples with more than ~250 crystals.

slope of the size distribution. Steeper distributions require larger total numbers of crystals, such that a sufficient number of crystals is observed in the larger size intervals; however, with increasing number of crystals, the number of small crystals increases very rapidly, making their analysis significantly more difficult and time-consuming, usually with very limited gain in data quality (e.g. compare 11% uncertainty with a sample size of ~425 crystals for the size fraction 20–40 μm with 8% uncertainty with 849 crystals, Sample F7-14B). What comes out of this discussion is that there is an intrinsic trade-off between the desired error in the largest size fraction and a manageable number of crystals in the smaller size intervals.

Consequently, to obtain crystal size distributions across a large spectrum of sizes, it becomes necessary to combine data obtained at various scales for a given rock specimen. We have used such an approach in our studies of the Bishop Tuff pumice clasts (Gualda *et al.*, 2004; Gualda & Rivers, 2006), and showed that the estimates obtained using tomographic data acquired at two scales agree very well for overlapping size intervals (Gualda & Rivers, 2006).

Although the discussion presented here is strictly applicable only to size distributions described by power laws, extension of the same rationale to other kinds of size distributions is rather straightforward. For the ubiquitous 'linear' size distributions (i.e. linear in a semi-log plot; see Marsh, 1998), the results would be very similar to those presented here, except that the number of large crystals would decrease more rapidly, and the number of small crystals would increase more slowly; the ideal approach would once again be to combine information obtained at various scales and resolutions. The most difficult case is certainly that of size distributions in which there is a reduction in the number of small crystals, especially that of lognormal or lognormal-like size distributions (Eberl *et al.*, 2002; Bindeman, 2005), in which case it becomes necessary to study large volumes at high resolution (Gualda *et al.*, 2004). In general, what is important is that, as long as the size distribution is not uniform (which seems to be always true for natural samples) there will be crystal-poor and crystal-rich size bins, and the researcher needs to take into consideration the intrinsic variations in uncertainty during experiment design and data analysis.

CONCLUSIONS

Crystal size distributions are obtained using a counting procedure; consequently, uncertainties related to counting statistics can be used as minimum estimates of error. Given that most natural samples are characterized by a decreasing number of crystals with increasing crystal size, uncertainties tend to increase markedly with crystal size, and the number of small crystals to be counted grows very quickly with increasing sample volume.

We used two tomographic datasets for early erupted Bishop Tuff pumice clasts to demonstrate this

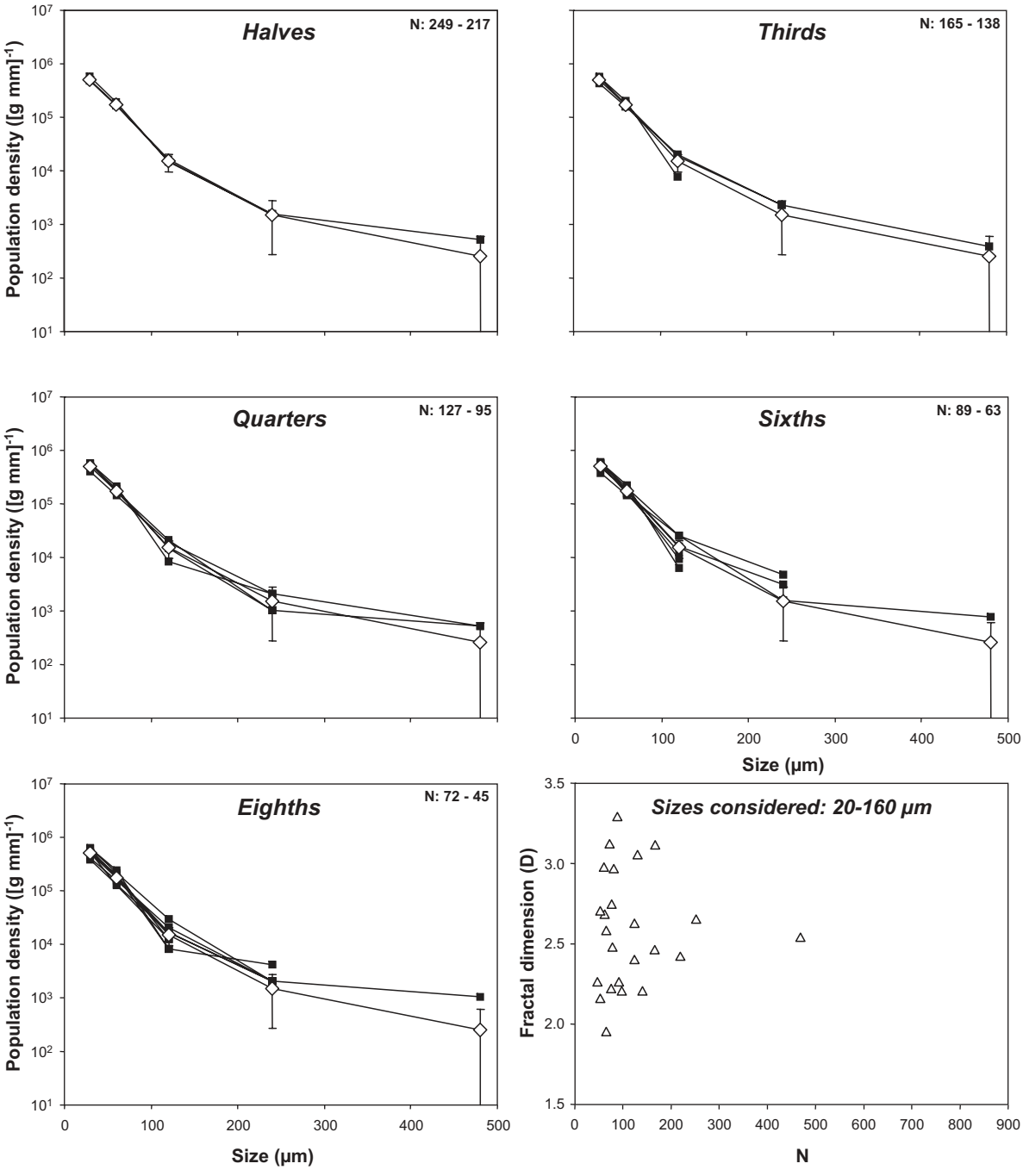

Fig. 9. Quartz size distribution plots obtained using subvolumes like those in Fig. 4 (first five panels), and fractal dimension (D) vs sample size (*N*) plot (bottom right panel) for sample F7-12B. Similarly to what happens with sample F7-14B, crystal size distributions with more than ~100 crystals adequately approximate the 'true' size distribution, the approximation being very good for subvolumes with more than ~250 crystals. Black squares correspond to the quartz size distributions obtained with the subvolumes. Open diamonds and error bars correspond to the size distribution obtained with the whole volume. Numbers in each diagram correspond to the range of total number of quartz crystals.

interplay between sample size and uncertainty associated with large size ranges. We demonstrate that with as few as 100 crystals in total, it is possible to properly estimate the population densities for small size bins in a sample. However, to obtain meaningful estimates across four bin sizes (a range of 20–320 μm), a total of at least ~250 crystals, but preferably more than 400 crystals is needed.

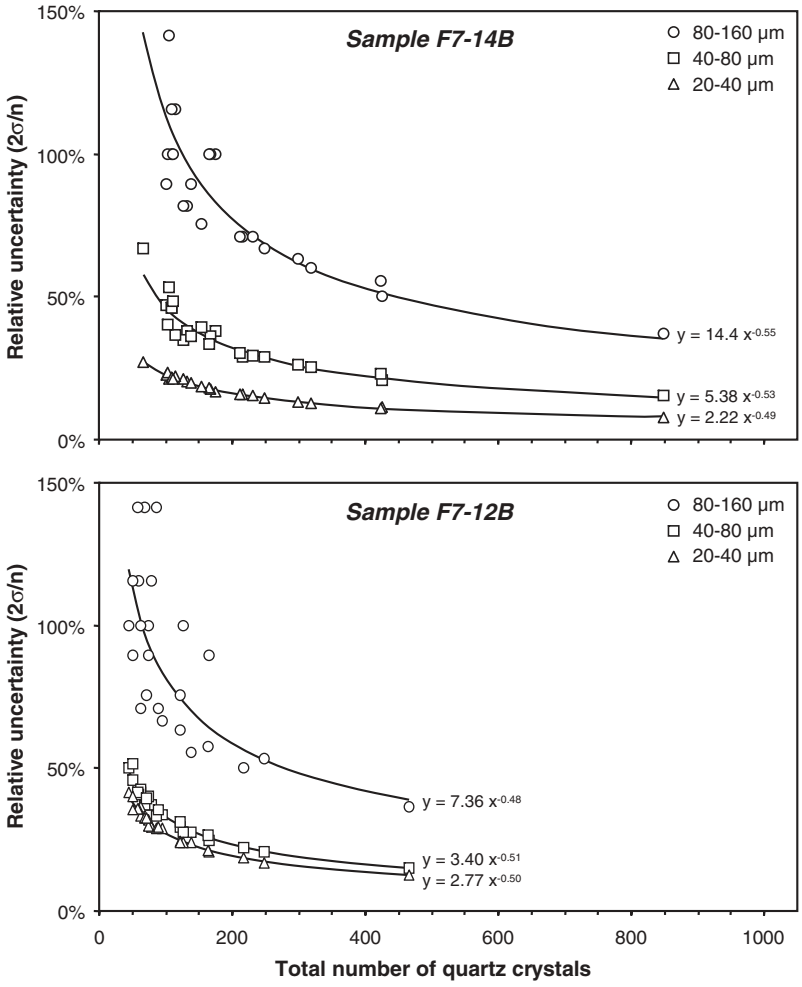

Fig. 10. Relative uncertainties vs total number of quartz crystals for the size fractions 20–40 μm, 40–80 μm, and 80–160 μm for samples F7-14B and F7-12B. Uncertainties are well approximated by power law equations with exponent close to −0·5, reflecting the fact that uncertainties are calculated as a function of counting statistics. Because the number of crystals in a given size range decreases dramatically with increasing crystal size, the uncertainties increase rapidly with increasing size range. To improve the statistics for the larger size fractions, the total number of crystals has to be increased, which results in a much greater increase in the number of smaller crystals, with no corresponding gain in data quality (note, for instance, the shallow slope of the curve for the size fraction 20–40 μm). Consequently, there is an intrinsic trade-off between the desired error in the largest size fraction and a manageable number of crystals in the smaller size intervals.

In most applications, it is necessary to limit the number of small crystals to a manageable number, which limits the maximum sample volume to be analyzed. Naturally, this effect is more dramatic for samples with steep crystal size distributions. In any case, this effect leads to a trade-off between sample volume and uncertainties on the larger size ranges. To avoid this problem (i.e. to limit errors to reasonable values for a large range of sizes) it becomes necessary to use multiple volumes (or sub-volumes) at variable spatial resolution.

For the two more readily available ways of obtaining 3D images of rocks, this trade-off between sample volume and spatial resolution is intrinsic to the data collection setup, either directly or indirectly. In the case of X-ray tomography, the spatial resolution is controlled by the sample volume because it is limited to the resolution of the imaging device (e.g. a CCD camera; see Gualda & Rivers, 2006). In the case of serial sectioning, a similar problem exists because the resolution is set mainly by the spacing between individual sections (see Mock & Jerram, 2005), which determines the number of steps necessary to characterize a given volume.

ACKNOWLEDGEMENTS

I am indebted to Mark Rivers for the continued support in developing applications of X-ray tomography to igneous petrology. This study emerged from communication with Alexander Mock, to whom I am grateful. Reviews

by Alexander Mock, Bruce Marsh, Michael Higgins, and Marjorie Wilson helped improve the manuscript and are much appreciated.

SUPPLEMENTARY DATA

Supplementary data for this paper are available at *Journal of Petrology* online.

REFERENCES

Anderson, A. T., Davis, A. M. & Lu, F. Q. (2000). Evolution of Bishop Tuff rhyolitic magma based on melt and magnetite inclusions and zoned phenocrysts. *Journal of Petrology* **41**, 449–473.

Bindeman, I. N. (2005). Fragmentation phenomena in populations of magmatic crystals. *American Mineralogist* **90**, 1801–1815.

Bryon, D. N., Atherton, M. P. & Hunter, R. H. (1995). The interpretation of granitic textures from serial thin sectioning, image-analysis and 3-dimensional reconstruction. *Mineralogical Magazine* **59**, 203–211.

Cashman, K. V. & Marsh, B. D. (1988). Crystal size distributions (CSD) in rocks and the kinetics and dynamics of crystallization. II: Makaopuhi lava lake. *Contributions to Mineralogy and Petrology* **99**, 292–305.

Castro, J. M., Cashman, K. V. & Manga, M. (2003). A technique for measuring 3D crystal-size distributions of prismatic microtites in obsidian. *American Mineralogist* **88**, 1230–1240.

Chayes, F. (1956). *Petrographic Modal Analysis*. New York: John Wiley, 113 pp.

Cooper, M. R. & Hunter, R. H. (1995). Precision serial lapping, imaging and three-dimensional reconstruction of minus-cement and post-cementation intergranular pore-systems in the Penrith Sandstone of north-western England. *Mineralogical Magazine* **59**, 213–220.

Denison, C. & Carlson, W. D. (1997). Three-dimensional quantitative textural analysis of metamorphic rocks using high-resolution computed X-ray tomography: Part II—Application to natural samples. *Journal of Metamorphic Geology* **15**, 45–57.

Eberl, D. D., Kile, D. E. & Drits, V. A. (2002). On geological interpretations of crystal size distributions: constant vs. proportionate growth. *American Mineralogist* **87**, 1235–1241.

Gualda, G. A. R. & Anderson, A. T., Jr (2005). Magnetite clusters on vesicle walls: evidence for pre-eruptive bubbles in the early-erupted Bishop Tuff, CA. *Geochimica et Cosmochimica Acta* **69**(10), A235.

Gualda, G. A. R. & Rivers, M. (2006). Quantitative 3D petrography using x-ray tomography: application to Bishop Tuff pumice clasts. *Journal of Volcanology and Geothermal Research* **00**, doi:10.1016/j.jvolgeores.2005.09.019.

Gualda, G. A. R., Cook, D. L., Chopra, R., Qin, L., Anderson, A. T., Jr & Rivers, M. (2004). Fragmentation, nucleation and migration of crystals and bubbles in the Bishop Tuff rhyolitic magma. *Transactions of the Royal Society of Edinburgh: Earth Sciences* **95**, 375–390.

Higgins, M. D. (2000). Measurement of crystal size distributions. *American Mineralogist* **85**, 1105–1116.

Howarth, R. J. (1998). Improved estimators of uncertainty in proportions, point-counting, and pass–fail test results. *American Journal of Science* **298**, 594–607.

Jerram, D. A., Cheadle, M. J., Hunter, R. H. & Elliott, M. T. (1996). The spatial distribution of grains and crystals in rocks. *Contributions to Mineralogy and Petrology* **125**, 60–74.

Ketcham, R. A. (2005). Computational methods for quantitative analysis of three-dimensional features in geological specimens. *Geosphere* **1**, 32–41.

Marsh, B. D. (1988). Crystal size distribution (CSD) in rocks and the kinetics and dynamics of crystallization: I—Theory. *Contributions to Mineralogy and Petrology* **99**, 277–291.

Marsh, B. D. (1998). On the interpretation of crystal size distributions in magmatic systems. *Journal of Petrology* **39**, 553–599.

Mock, A. & Jerram, D. A. (2005). Crystal size distributions (CSD) in three dimensions: insights from the 3D reconstruction of a highly porphyritic rhyolite. *Journal of Petrology* **46**, 1525–1541.

Pallister, J. S., Hoblitt, R. P., Meeker, G. P., Knight, R. J. & Siems, D. F. (1996). Magma mixing at Mt Pinatubo: petrographic and chemical evidence from 1991 deposits. In: Newhall, C. G. & Punongbayan, R. S. (eds) *Fire and Mud: Eruptions and Lahars of Mt. Pinatubo, Philippines*. Seattle, WA: University of Washington Press, pp. 687–732.

Petford, N., Davidson, G. & Miller, J. A. (2001). Investigation of the petrophysical properties of a porous sandstone sample using confocal scanning laser microscopy. *Petroleum Geoscience* **7**, 99–105.

Rivers, M. L., Sutton, S. R. & Eng, P. (1999). Geoscience applications of x-ray computed microtomography. *Proceedings of SPIE, Developments in X-Ray Tomography II* **3772**, 78–86.

Sahagian, D. L. & Proussevitch, A. A. (1998). 3D particle size distributions from 2D observations: stereology for natural applications. *Journal of Volcanology and Geothermal Research* **84**, 173–196.

Wallace, P. J., Anderson, A. T., Jr & Davis, A. M. (1999). Gradients in H_2O, CO_2, and exsolved gas in a large-volume silicic magma system: interpreting the record preserved in melt inclusions from the Bishop Tuff. *Journal of Geophysical Research—Solid Earth* **104**, 20097–20122.

Wilson, C. J. N. & Hildreth, W. (1998). The Bishop Tuff: new insights from eruptive stratigraphy. *Journal of Geology* **105**, 407–439.